



Fast and novel multiwalled carbon nanotubes decorated with metal oxide nanoparticles for potentiometric detection of a prohibited medication in sports acebutolol hydrochloride

Amal M. Al-Mohameed^a, Suliman Y. Al Omar^{b,*,**}, Maha F. El-Tohamy^{a,*}

^a Department of Chemistry, College of Science, King Saud University, P.O. Box 22452, Riyadh, 11495, Saudi Arabia

^b Doping Research Chair, Zoology Department, College of Science, King Saud University, Riyadh University, Riyadh, 11451, Saudi Arabia

ARTICLE INFO

Keywords:

Abused drugs
Acebutolol hydrochloride
Multiwalled carbon nanotubes
Functionalized sensor
Metal oxide nanostructures
Lavandula spica flowers

ABSTRACT

A straightforward approach for creating fast and novel potentiometric sensors that are modified with multi-walled nanotubes (MWCNTs) was described. The impact of the selective sensor's material was studied. The suggested sensors were successfully fabricated for instant and fast detection of the prohibited β -adrenoreceptor blocking agent acebutolol hydrochloride (AC) in commercial products. Acebutolol-phosphomolybdate (AC-PM) carbon paste sensor was formed by mixing AC and phosphomolybdic acid and graphite powder in the presence of *o*-nitrophenyl octyl ether (*o*-NPOE) as a plasticizing agent. The functionalized AC-PM-MWCNTs and AC-PM-MWCNTs- Al_2O_3 nanocomposite sensors were prepared and all parameters affecting the sensors' potential responses have been investigated as well as the green synthesis of Al_2O_3 NPs has been characterized using various microscopic and spectroscopic techniques. AC-PM-MWCNTs and AC-PM-MWCNTs- Al_2O_3 nanocomposite sensors demonstrated linearity of 1.0×10^{-7} - 1.0×10^{-2} and 1.0×10^{-8} - 1.0×10^{-2} mol L⁻¹, respectively with regression equations $-53.571x + 423.24$ ($r = 0.999$) and $-57.107x + 518.54$ ($r = 0.999$). It also revealed excellent selectivity and sensitivity for the determination and quantification of AC. The developed potentiometric system was suitable for the determination of AC in bulk powder and commercial products.

1. Introduction

Doping is currently a serious problem in sports physiology on a global scale. In addition to physical issues, this also has moral and ethical implications for the integrity of teamwork in athletic competition [1]. This has a direct impact on international sporting events. Any type of behavior that encourages the use of particular medicines for the purpose of enhancing athletic performance or endurance is referred to as doping [2]. The International Olympic Committee deems this situation to be illegal and immoral. These committees frequently accuse such situations that occasionally occur of severe regular actions. This group consistently makes enormous efforts to promote doping-free sports [3].

Beta-blockers are frequently prescribed for cardiovascular problems. They largely lower mean arterial pressure, heart rate, cardiac output, and stroke volume. usage has increased for the treatment of hypertension and after myocardial infarction. When a soothing

* Corresponding author.

** Corresponding author.

E-mail addresses: muhemeed@ksu.edu.sa (A.M. Al-Mohameed), syalomar@ksu.edu.sa (S.Y. Al Omar), moraby@ksu.edu.sa (M.F. El-Tohamy).

effect is necessary during sporting events, such as during shooting competitions for archery, beta-blockers are utilized. Beta-blockers have a tendency to prevent maximum performance in events that need an enhancement in cardiac response. They are not utilized to enhance performance in aerobic activities. The main advantages are anxiety reduction and tremor relief. However, inadequate glucose management in people with diabetes mellitus, bronchospasm, heart failure, and heart block, as well as weariness and a reduced capacity for endurance activity, are some of the adverse effects [4].

Acebutolol hydrochloride (AC), is a hydrophilic β -adrenoreceptor blocker with mild intrinsic sympathomimetic action that is used to treat ventricular arrhythmias and hypertension in individuals [5].

Several analytical techniques have been reported for the separation and quantification of AC in various analytical samples. Different thin-layer chromatographic separation approaches have been developed for enantioresolution of acebutolol [6]. LC-MS/MS investigation for the identification and confirmation of degradation products of acebutolol has been developed by Jithavech et al. [7]. Recently, a molecular interaction of AC with serum albumin has been studied using a combined calorimetric and spectroscopic approach [8]. Few electrochemical methods have been published for the determination of AC in pharmaceutical products and bio-samples [9–12]. Although bomb calorimeters in labs are insulated to reduce heat loss, it is difficult to eliminate all heat loss. Furthermore, the reactants in the calorimeter may not be well-mixed, resulting in uneven heating and an additional source of inaccuracy in your readings [13]. In addition, the electrochemical approaches have certain limitations, they cannot be recycled, can leak (weak acid electrolyte interacts with zinc), has a limited shelf life, unpredictable voltage and current (as the battery goes down), and produces little power [14].

Since the publication of the first study on the elimination of internal solutions more than 40 years ago, all-solid-state potentiometric sensors have attracted significant scientific attention [15]. Practical application needs were the driving force behind the search for internal-solution-free potentiometric sensors, where simplicity, cheap cost, and little maintenance are obvious advantages. The use of transducer layers positioned between the metallic support and ion-selective membrane allows for the successful elimination of internal solution, which is understood as achieving sensors with analytical parameters that are well comparable with those of classical (internal solution containing) counterparts and, more importantly, of similar stability of potential readings over time [16]. The usual toolkit for reliable and exact determination of diverse species in biological and industrial studies now includes potentiometric approaches using potentiometric sensors [17].

In fact, utilizing certain species to modify the sensor composition chemically or physically can increase the sensitivity and selectivity of carbon paste sensors (CPSs). The altering elements can be included in the paste right away [18] or they can be adsorbed onto the sensor surface [19].

Carbon nanotubes (CNTs) have increased in popularity since 1991 [20]. Numerous distinctive characteristics of these nanotubes include their metallic or semi-metallic behavior, extremely low weight, high thermal conductivity, mechanical strength, surface area, and electrical conductivity [21]. The distinct electronic characteristics suggest that this substance can facilitate a more efficient electronic transfer, leading to a wider range of applications in electrochemistry [22]. CNTs, on the other hand, have two fundamental drawbacks: bundling and limited dispersibility. This is mostly due to the van der Waals forces produced between the CNTs, which cause agglomeration processes and bundle formation, making it very difficult to obtain excellent dispersion in any solvent [23]. Better dispersion efficiency and non-aggregation are still challenges that can be enhanced and attained by functionalizing the surface of CNTs. The electrical conductivity of CNTs is a parameter that needs to be improved regardless of its practical application. Decoration of the outer surface of carbon nanotubes (CNTs) with metallic nanoparticles (NPs) has proven to be a viable and interesting way to improve the performance of electrical devices and sensors for a variety of electrochemical applications [24].

Transitional metal oxide nanoparticles such as titanium oxide (TiO_2 NPs), zinc oxide (ZnONPs), aluminum oxide (Al_2O_3 NPs), and nickel oxide (NiONPs), etc. are an important category of inorganic nanostructures that have been commonly tested due to their attractive catalytic, electronic and magnetic features compared to their bulk form [25]. Among these metal oxides, Al_2O_3 NPs is a promising dielectric semiconductor nanomaterial, which has been a focus of sensors and electrochemical instruments due to its potential sensing applications [26]. Nanomaterials can be created using a variety of physical and chemical techniques [27–29]. According to the findings, these techniques have a number of drawbacks, including the use of costly and toxic stabilizers or capping agents, toxic organic solvents or hazardous materials, higher temperatures necessary for final product processing, and more [30]. As a result, researchers are interested in creating green methods for nanomaterial synthesis [31].

The functionalization of MWCNTs with metal oxides has been suggested with promising findings to progress the sensitivity and selectivity of chemical sensors [32]. The current work suggests the fabrication of a simple and novel MWCNTs- Al_2O_3 decorated sensor for the determination of AC as one of the most important prohibited beta-adrenoreceptor blocker medications in sports in its authentic and commercial products. The synthesized nanomaterials and the resulting nanocomposite were fully characterized with spectroscopic and microscopic techniques. All effective experimental parameters were investigated and optimized. Moreover, the validity and suitability of the new disposable sensor were investigated with respect to the previously recommended guidelines for analytical method requirements.

2. Experimental

2.1. Chemicals

All chemicals, reagents, and solvents used in this study were of high purity. The Milli-Q water obtained from Milli-Q lab instrument was used for the preparation of all solutions. Multi-walled carbon nanotubes with the specification of (20–30 nm OD, $\sim 30 \mu\text{m}$ length, 1.23 w% COOH content, > 95 w% purity), Aluminum (III) nitrate nonahydrate ($\text{Al}(\text{NO}_3)_3 \cdot 9\text{H}_2\text{O}$, 99.9 %), ethylene glycol (99.8 %),

nitric acid (70 %), hydrochloric acid (37 %), citric acid (≥ 99.5 %), di-octylphthalate (DOP, ≥ 97.0 %), dibutylsebacate (DBS, ≥ 97.0 %), and *ortho*-nitrophenyl octyl ether (*o*-NPOE, ≥ 97.0 %) were purchased from Sigma Aldrich (Hamburg, Germany). Pure olive oil and paraffin oil were purchased from local stores, in Riyadh, Saudi Arabia.

2.2. Plant material

In this investigation, dried *Lavandula spica* flowers of Saudi Arabia origin were employed. The moisture content of the flowers was evaluated by drying to a constant mass at 100 ± 5 °C and was less than 2 %. The flowers were pulverized in a grinder (GT11, Tefal, Rumilly, France) and stored at ambient temperature in a glass jar until use.

2.3. Instruments

The analytical detections were performed using a simple and novel fabricated potentiometric MWCNTs- Al_2O_3 nanocomposite sensor in connection with a silver/silver chloride reference electrode. HANNA-211 device (Smithfield, Rhode Island, United States) was used for measuring all potential difference readings. In order to optimize the pH throughout the experiment Metrohm-744 (Herisau, Switzerland) pH-meter was used. Various characterization techniques were utilized to confirm the synthesis of Al_2O_3 NPs and functionalized MWCNTs- Al_2O_3 nanocomposite, including JSM-7610 F scanning electron microscope (SEM, Tokyo, Japan), Perkin-Elmer-spectrometer (Waltham, United States), 2600i-Shimadzu-spectrophotometer (Kyoto, Japan), 6000- X-ray Shimadzu diffractometer (Kyoto, Japan). The surface mapping and elemental constituents in the prepared Al_2O_3 NPs and functionalized MWCNTs- Al_2O_3 nanocomposite sample were tested by Energy-Dispersive X-Ray Spectroscopy (EDX, Tokyo, Japan). Thermogravimetric instrument (TGA801 thermogravimetric analyser, Dubai, United Arab Emirates).

2.4. Preparation of *Lavandula spica* flowers extract

Lavandula spica flowers were washed with Milli-Q water, kept to dry in the air overnight, and finely powdered. About 10 g powder of flowers were suspended well in 200 mL of Milli-Q water and kept under constant agitation at 80 °C for 2 h. The resulting extract was cooled to 25 °C, centrifuged at 6000 rpm for 5 min, and then filtered through Fisherbrand™ filter paper 55 (2–3 μm pore size). The final extract was stored at 4 °C in a refrigerator for further use in the synthesis of Al_2O_3 NPs (Scheme 1).

2.5. Synthesis of Al_2O_3 NPs using *Lavandula spica* flowers extract

To synthesize Al_2O_3 NPs, a slight modification of the technique [33]. was conducted by magnetically stirring 10 mL of extract and 50 mL of aluminum nitrate (2.0 mol L^{-1}) for 25–30 min at 80 °C. A few drops of sodium hydroxide (0.2 mol L^{-1}) were added dropwise to the above mixture. The resulting Greenish-brown precipitate of Al_2O_3 NPs was then centrifuged at 3500 rpm for 5 min, filtered using Fisherbrand™ filter paper (2–3 μm pore size), dried, and stored in a container for future experiments. A stock solution of Al_2O_3 NPs was made by dissolving 0.1 g of each nanopowder in 100 mL deionized water, sonicating for 10 min, and refrigerating at 4 °C (Scheme 2a). The phytochemical components in the plant extract play a crucial role in the synthesis of nanomaterials as they act as reducing, capping, and stabilizing agents.

2.6. Synthesis of MWCNTs decorated with Al_2O_3 NPs

The synthesis of MWCNTs decorated with Al_2O_3 NPs was conducted using a typical wet-impregnated procedure [34]. The purification of MWCNTs was first performed from any remaining catalyst by washing with a 5 mol L^{-1} HCl solution, after which the surface of the tubes was functionalized and opened by oxidation with a nitric acid solution (65 %) and reflux for 6 h. Finally, the treated MWCNTs were washed with Milli-Q water several times until the pH reached 7, and then they were dried at 90 °C for an overnight period. For the functionalization step, approximately 10 mL of Al_2O_3 NPs (1.0 w%) was suspended in Milli-Q water and added to the previously acid-treated MWCNTs dispersed in Milli-Q water and sonicated for 2 h, and the mixture was magnetically stirred for another 2 h at ambient temperature, then ammonia solution was added dropwise to neutralize the pH to 7. To evaporate the solvent the temperature was elevated to 80 °C. Finally, the dried mixture was calcined for 4 h at 350 °C (Scheme 2b).



Scheme 1. Schematic illustration of *Lavandula spica* flowers extraction steps.



Scheme 2. (A) Preparation steps of Al₂O₃NPs and (b) functionalization of MWCNTs with Al₂O₃NPs using direct wet impregnation method.

2.7. Characterization of synthesized Al₂O₃NPs and MWCNTs-Al₂O₃ nanocomposite

The synthesized Al₂O₃NPs and MWCNTs-Al₂O₃ nanocomposite were characterized with respect to its optical behavior, possible functional groups present during the synthesis process, crystallinity and shape, average crystallite size, surface morphology and elemental composition by various optical devices including (UV-vis spectroscopy, FT-IR spectroscopy, and XRD spectroscopy) and microscopic devices such as SEM connected with EDX detection. XRD diffraction pattern of MWCNTs-Al₂O₃NPs nanocomposite was recorded to evaluate the nanocomposite nature using Cu K α radiation source at $\lambda = 0.154$ nm in the range of 2θ from 10° to 80° . The thermal stability of the formed nanocomposite was investigated by thermogravimetric analysis at a heating range from 30°C to 600°C and a rate of heating of $10^\circ\text{C}/\text{min}$ in air. The morphological structure of the nanocomposite surface was examined under SEM. Prior to the examination, the sample dust was spread out on conductive carbon tape and coated with a 5 nm thick coating of platinum (Quorum sputter coater model: Q150R S). The images were picked at an acceleration voltage of 15 kV and $30,000\times$ magnification. In order to determine the elemental makeup of both Al₂O₃NPs and synthetic MWCNTs nanocomposite, energy dispersive X-ray (EDX) analysis was also carried out.

2.8. Preparation of electroactive material

The electroactive material (AC-PM) was obtained by slow mixing of 50 mL of AC (1.0×10^{-2} mol L⁻¹) solution with the same quantity of phosphomolybdic acid (1.0×10^{-2} mol L⁻¹) solution under constant magnetic stirring of 450 rpm for 20 min. The formed yellowish-green precipitate was collected by filtration through a Fisherbrand™ grade 55 filter paper (pore size 2–3 μm), remove the chloride by washing it three times with Milli-Q water. To ensure the free precipitate from chloride, it was tested using silver nitrate solution and then dried overnight at ambient temperature and finely powdered. The elemental analysis of AC-PM revealed the formation of 1: 1 of the [C₁₈H₂₉N₂O₄:PMo₂O₄₀] ion-pair.

2.9. Construction of modified MWCNTs and functionalized MWCNT-Al₂O₃ nanocomposite sensors

The modified carbon paste sensor with MWCNTs was constructed manually by mixing graphite powder with *o*-NPOE, electroactive material AC-PM, (60:30:10 w/w/w) and MWCNTs (55: 25: 10: 10 w/w/w/w) in a mortar to produce AC-PM-MWCNTs carbon paste sensor. The modified AC-PM-MWCNT-Al₂O₃ nanocomposite sensor was prepared by mixing (55: 25: 10: 10 w/w/w/w) graphite powder, *o*-NPOE, electroactive complex AC-PM, and MWCNT-Al₂O₃ nanocomposite, respectively. The resulting mixture was hand blended until the formation of a homogeneous paste. The resulting paste was then packed in the body of the sensor with an internal radius of 2.2 mm and the surface of the sensor was polished using filter paper to obtain a shiny and smooth surface. A copper wire was used for the electrical connection. The constructed sensors were preconditioned in 1.0×10^{-3} mol L⁻¹ AC solution.

2.10. Conductometric investigation

Conductometric titration was conducted using a Jenway-4520 Conductivity meter. The measurements were performed by titrating 5.0 of AC (1.0×10^{-2} mol L⁻¹) with PM solution (1.0×10^{-2} mol L⁻¹). Following each edition of the titrant, the conductance of the solution was measured. The conductance versus molar ratio titration plot revealed a break that is consistent with the stoichiometry of

the electroactive ion-pair.

2.11. Preparation of analytical samples

2.11.1. Preparation of AC authentic samples

A standard solution of authentic AC was prepared using 0.37 g dissolved in 100 mL Milli-Q water to obtain $1.0 \times 10^{-2} \text{ mol L}^{-1}$. The desired analytical concentrations were prepared from the above standard solution by serial dilution using the same solvent.

2.11.2. Preparation of SECTRAL® samples

The samples of SECTRAL® tablets (200 mg acebutolol hydrochloride/tablet) were conducted by weighing 10 tablets and grounding them to fine powder. An equivalent weight to prepare $1.0 \times 10^{-2} \text{ mol L}^{-1}$ was dissolved in 50 mL distilled water centrifuged using 6000 rpm for 10 min and filtered using Whatman filter paper No.4. the filtrate was completed to 100 mL using distilled water. serial working solutions were prepared for analyses using the same solvent. As previously stated, these solutions were tested using functionalized AC-PM-MWCN and AC-PM-MWCNTs- Al_2O_3 nanocomposite sensors by direct calibration approach.

Meanwhile, the serum samples were prepared using 1.0 mL of commercial serum spiked with suitable concentrations of AC (1.0×10^{-7} - $1.0 \times 10^{-2} \text{ mol L}^{-1}$) and placed into a series of centrifuge tubes. Each tube was then filled with 10 mL of diethyl ether and spun at 3500 rpm for 5 min. The deproteinized layer was then transferred to a 100-mL measuring flask and filled with distilled water to attain its capacity. As previously stated, these solutions were tested using the functionalized AC-PM-MWCNTs- Al_2O_3 nanocomposite sensor by direct calibration approach.

2.12. Calibration graph

The linear relationships between AC concentrations and the potential readings of the suggested AC-PM-MWCNTs and AC-PM-MWCNTs- Al_2O_3 nanocomposite sensors were plotted using 1.0×10^{-7} - 1.0×10^{-2} and 1.0×10^{-8} - $1.0 \times 10^{-2} \text{ mol L}^{-1}$ of AC standard samples.

3. Results and discussion

3.1. Characterization of synthesized Al_2O_3 NPs and MWCNTs- Al_2O_3 NPs nanocomposite

Ultraviolet and visible (UV-Vis) absorption spectroscopy is an excellent technique for measuring the attenuation of light as it travels through a sample under investigation or after reflection from the sample. Both portions of light (UV and Vis) are active and can excite electrons to higher energy levels [35]. At room temperature, optical investigations of MWCNTs, pre-synthesized Al_2O_3 NP, and MWCNTs- Al_2O_3 nanocomposite were carried out in the wavelength range 200–600 nm. A comparative UV-visible spectroscopy investigation of *Lavandula spica* flowers extract absorption spectra (Fig. 1) with MWCNTs, the green synthesized Al_2O_3 NP, and MWCNTs- Al_2O_3 nanocomposite shows that the plant flowers extract has various peaks at 255, 340, and 420 nm, whereas the MWCNTs, Al_2O_3 NP, and MWCNTs- Al_2O_3 nanocomposite samples produced single sharp peaks at 270, 265, and 300 nm for the three mentioned samples, respectively.

The electrical and optical band gaps behavior of MWCNTs, Al_2O_3 NP, and MWCNTs- Al_2O_3 nanocomposite can be assessed by studying its UV-visible absorption spectrum features. The band gap energy of each investigated sample was calculated using the

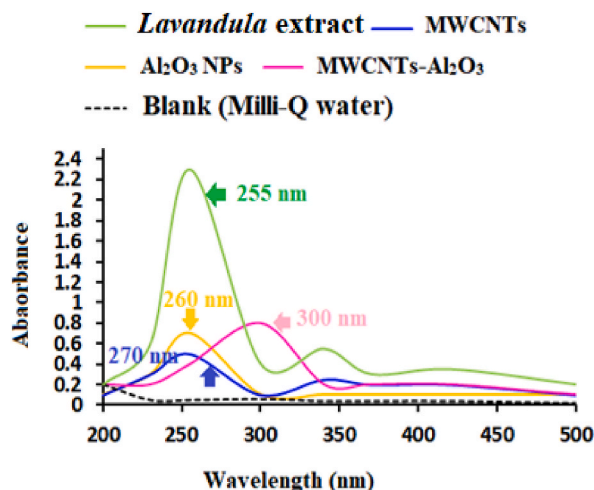


Fig. 1. Optical UV-vis spectra of *Lavandula spica* flowers extract, MWCNTs, Al_2O_3 NPs, MWCNTs- Al_2O_3 nanocomposite.

energy quantum mechanics equation and the band gap energy E_g was estimated from equation (1):

$$E_g = hc/\lambda \quad (1)$$

Where these values represented the band gap (E_g), bank constant, 6.626×10^{-34} J s (h), C velocity of light, 2.99×10^8 m/s (C), and absorption band value (λ), respectively. The conversion factor 1 eV is equivalent to 1.6×10^{-19} J. The optical band gap of Al_2O_3 NPs was found to be 4.77 eV and this value is less than that of the bulk due to the presence of oxygen vacancies and point defects [36]. However, the band gap values of MWCNTs and MWCNTs- Al_2O_3 nanocomposite samples were estimated as 4.59 eV and 4.13 eV, respectively. The surface plasmon resonance (SPR) offers the surface a reduced form while also increasing scattering possibility and radiation penetration. These mechanisms, which involve the surface-level production of holes and the separation of electrons, speed up the oxidation process. Furthermore, alterations to the dielectric matrix have been demonstrated to influence the absorbance peak visible on an SPR. The effective dielectric behavior of the matrix is known to be intimately connected to its refractive index [37].

FT-IR technique was applied to study the functional groups that were present in the prepared samples. The FT-IR spectrum of MWCNTs (Fig. 2a) showed three peaks at 3417, 2924, and 2338 cm^{-1} corresponding to medium O-H stretching vibration group, medium C-H stretching vibration group, and strong O=C=O carbon dioxide stretching vibration. The absorption peaks at 1622 and 1562 cm^{-1} correspond to medium C=C stretching conjugated aromatic structure. Whereas, the absorption peaks at 1102 and 613 cm^{-1} correspond to strong C-O stretching vibration and strong stretching vibration of Cl-C halo compound from the activation of MWCNTs using hydrochloric acid. These values matched the previously addressed values in the literature [38]. The FT-IR of Al_2O_3 NPs prepared by *Lavandula spica* flowers extract showed many remarkable absorption peaks at 3444, 2433, 2098, 1636, 1358, 1049, 985, 834, and 615 cm^{-1} corresponding to a strong intermolecular O-H stretching vibration, medium N-H stretching vibration of a primary amine, medium stretching C=C of alkene, medium C-H bending of alkane, strong C-O stretching of primary alcohol, strong C=C bending of alkene, medium C=C bending trisubstituted alkene, and Al-O stretching vibration, respectively (Fig. 2b). Fig. 2c showed the FT-IR spectrum of *Lavandula spica* flowers extract and four peaks were observed at 3418 (strong broad O-H of phenolics), 2928 (strong N-H stretching of amine salts), 2367 cm^{-1} (strong O=C=O carbon dioxide), and 2125 (strong stretching N=N=N of azide), respectively. Moreover, others appeared in 1738, 1638, 1378, and 1261 cm^{-1} . These peaks are attributed to strong C=O stretching of conjugated anhydride, medium C=C stretching of conjugated alkene, medium O-H bending of phenol, and medium O-H bending of carboxylic acid, respectively. The absorption peak at 1055 cm^{-1} was due to the presence of C-O stretching vibration of primary alcohol and the peaks at 615 and 477 cm^{-1} were due to the presence of halo compounds. Furthermore, the recording FT-IR spectrum of MWCNTs- Al_2O_3 nanocomposite (Fig. 2d) displayed the presence of the same absorption peaks at 3460, 2365, 2091, 1625, 1515, 1056, 837, 613, and 420 cm^{-1} due to the presence of a strong intermolecular O-H stretching vibration, strong O=C=O stretching of carbon dioxide, medium stretching C=C of alkene, medium C-H bending of alkane, strong N-O stretching of the nitro compound, C-O stretching vibration of primary alcohol, medium N-H stretching of a primary amine, halo, and Al-O vibration peaks. The observed peaks appeared as in the three previously discussed spectra with slight modification revealing the formation of MWCNTs- Al_2O_3 nanocomposite [39].

XRD measurement revealed the crystallinity and plane of MWCNTs. The XRD pattern of pure carbon nanotubes was depicted in Fig. 3a, with diffraction peaks at 25.42° and 43.53° corresponding to (002) and (100) reflection planes, respectively, which were indexed to the hexagonal graphite peak for carbon nanotubes (JCPDS No. 41-1487). Furthermore, the pattern showed that the XRD pattern of MWCNTs displayed a high degree of crystallinity and a low quantity of amorphous carbon and impurities [40].

The XRD patterns of the green synthesized Al_2O_3 NPs using *Lavandula spica* flower extract revealed the presence of several significant peaks at 22.82° (0 1 2), 26.62° (0 1 4), 29.39° (1 1 0), 35.38° (1 0 4), 38.95° (1 1 0), 42.51° (1 1 3), 52.66° (0 2 4), 56.46° (1 1 6), and 63.49° (1 2 2) crystalline planes (Fig. 3b). The recorded results matched the standard crystalline JCPDS Card no. 71-1123 for aluminum oxide nanoparticles [41]. The average crystalline shape of the prepared MWCNTs- Al_2O_3 nanocomposite was demonstrated in Fig. 3c. Two XRD peaks at 25.42° and 43.53° corresponding to (002) and (100) reflection planes of carbon nanotubes were observed.

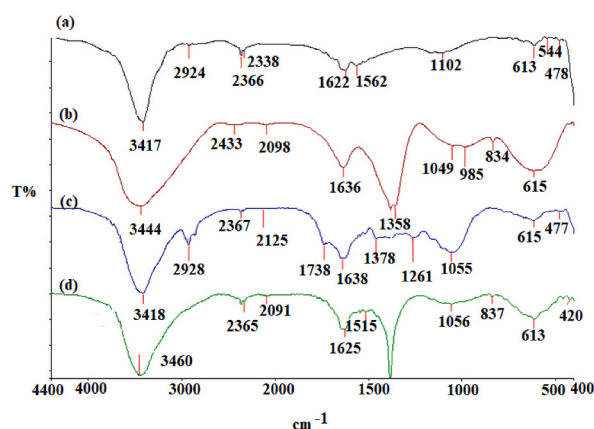


Fig. 2. FT-IR spectra of (a) MWCNTs, (b) Al_2O_3 NPs, (c) *Lavandula spica* flowers extract, and (d) MWCNTs- Al_2O_3 nanocomposite.

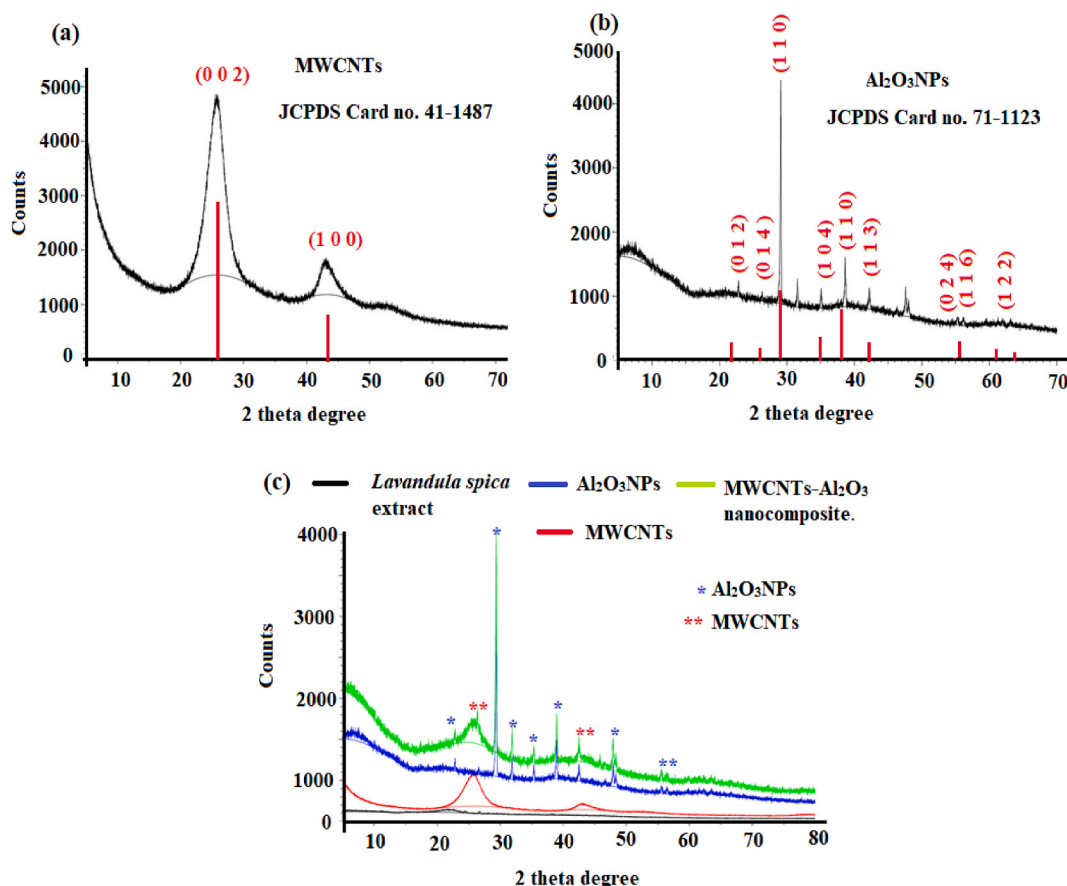


Fig. 3. XRD patterns of (a) MWCNTs, (b) Al₂O₃NPs synthesized using *Lavandula spica* flowers extract, (c) Comparative XRD spectra of *Lavandula spica*, MWCNTs, Al₂O₃NPs and MWCNTs-Al₂O₃ nanocomposite.

Furthermore, all peaks recognized by the blue star expressed the crystalline planes of Al₂O₃NPs confirming the functionalization of MWCNTs surface with Al₂O₃NPs (Fig. 3c). Also, it is important to notice in Fig. 3c that the XRD spectrum of *Lavandula spica* flowers displayed peaks at 2θ degrees 15.06–26.73° revealing the presence of phytochemical components containing carbon.

The average crystallite size in each green-produced nanomaterial was estimated using Debye-Scherrer's relation equation (2) [42].

$$D = 0.94\lambda/\beta\cos\theta \quad (2)$$

Where the average crystallite size (D), the absorption wavelength 1.54056 for Cu K radiation (λ), a constant value (0.94), the peak breadth at 1/2 maximum intensity (β), and the peak position angle (θ), respectively. The computed values for MWCNTs, Al₂O₃NPs, and MWCNTs-Al₂O₃ nanocomposite were 17.7 ± 1.4, 17.9 ± 0.9, and 18.5 ± 1.2 nm, respectively. No additional peaks in the recorded

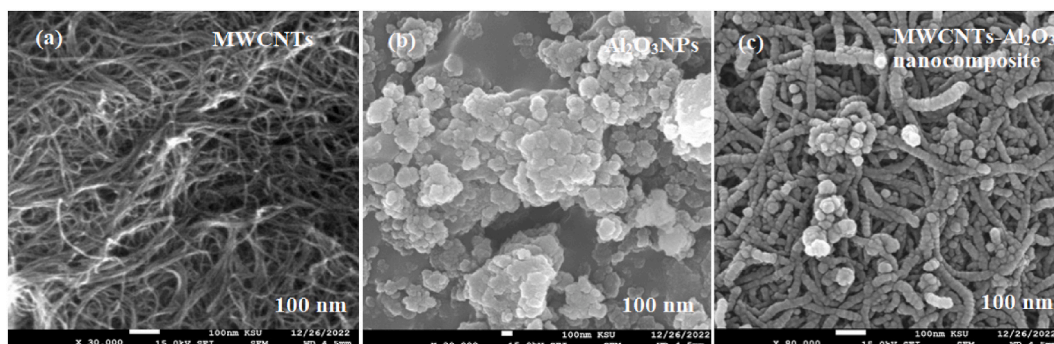


Fig. 4. SEM micrographs of (a) MWCNTs, (b) Al₂O₃NPs, and (c) MWCNTs-Al₂O₃ nanocomposite.

spectrum indicate excellent free impurities synthesized nanomaterials.

SEM was applied to investigate the morphological shape and size of MWCNTs, Al_2O_3 NPs, and MWCNTs- Al_2O_3 nanocomposite (Fig. 4). The depicted images showed that the MWCNTs exhibited tube-like shapes with homogeneous distribution, while Al_2O_3 NPs appeared as agglomerated spherical particles. In the image of MWCNTs- Al_2O_3 nanocomposite, it was clear that the Al_2O_3 NPs were successfully uploaded on the surface of MWCNTs producing the nanocomposite. In the three samples, the particle size was around 100 nm (Fig. 4a–c).

The elemental composition of MWCNTs, Al_2O_3 NPs, and MWCNTs- Al_2O_3 nanocomposite was conducted using SEM connected with an EDX spectrometer. According to the obtained results, it was noticed that the EDX spectrum of MWCNTs showed a weight% of 73.56 % and 26.35 % for C and O, respectively (Fig. 5a). Whereas, in the spectrum of the Al_2O_3 NPs sample the weight% of Al and O were 78.52 % and 21.48 %, respectively (Fig. 5b). EDX analysis of the MWCNTs- Al_2O_3 nanocomposite exhibited weight % of 63.16 %, 32.24 %, and 13.6 % for C, O, and Al, respectively (Fig. 5c). The elemental mapping of the above-mentioned nanomaterials was also investigated to show the elemental distribution of the nanomaterials and the morphological surfaces of MWCNTs, Al_2O_3 NPs, and MWCNTs- Al_2O_3 nanocomposite were shown in Fig. 6a–c.

3.2. Elemental analysis of electroactive complex

The electroactive ion-pair AC: PM was characterized by elemental analysis. The obtained data revealed the formation of an AC: PM ion-pair with a 1: 1 stoichiometric ratio. The calculated values were found to be C = 18.01 %, H = 2.44 %, N = 2.33 %, and O = 58.65 %. However, the found values were C = 17.99, H = 2.21, N = 2.26, and O = 58.62, respectively. The obtained results were in

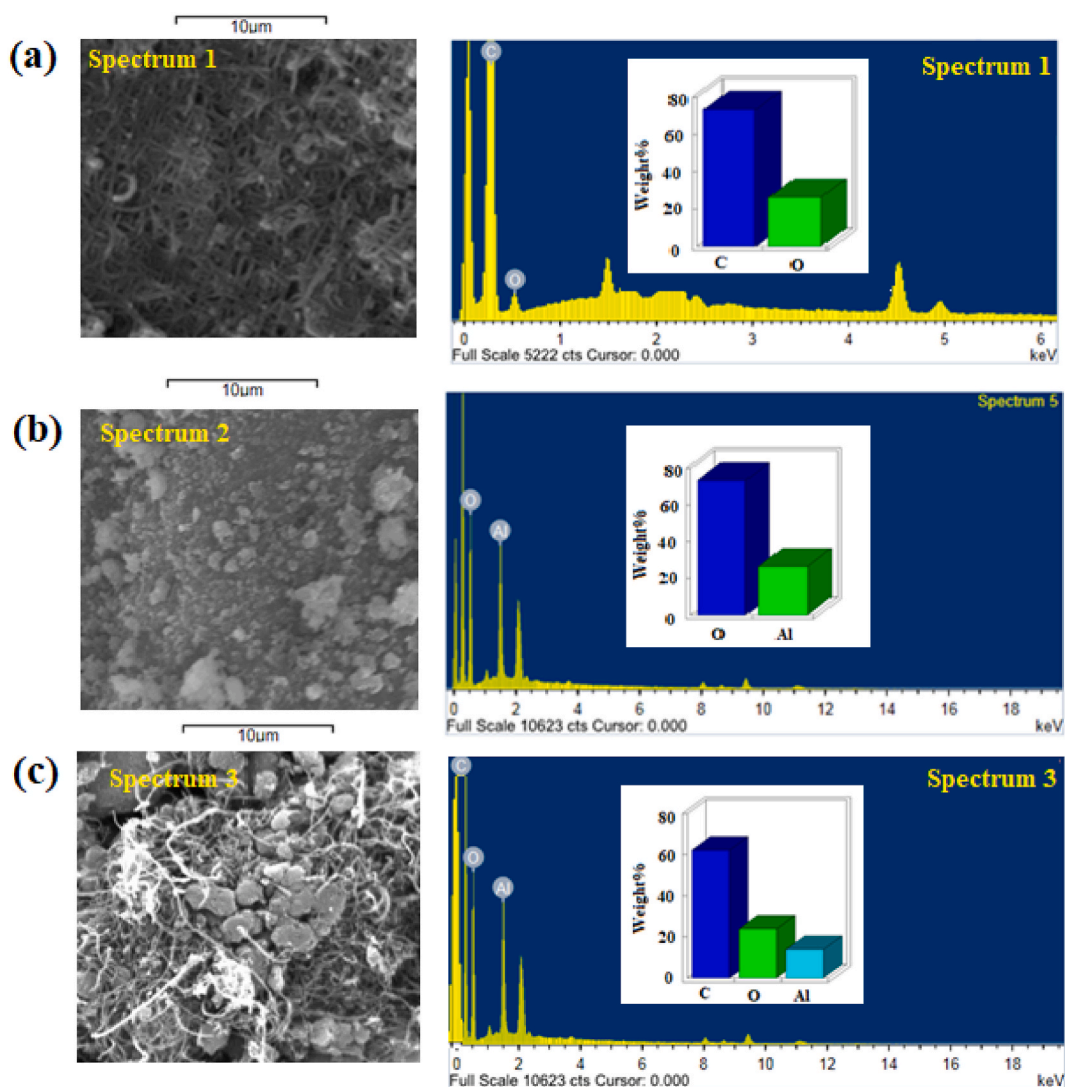


Fig. 5. SEM and EDX images of (a) MWCNTs, (b) Al_2O_3 NPs, and (c) MWCNTs- Al_2O_3 NPs.

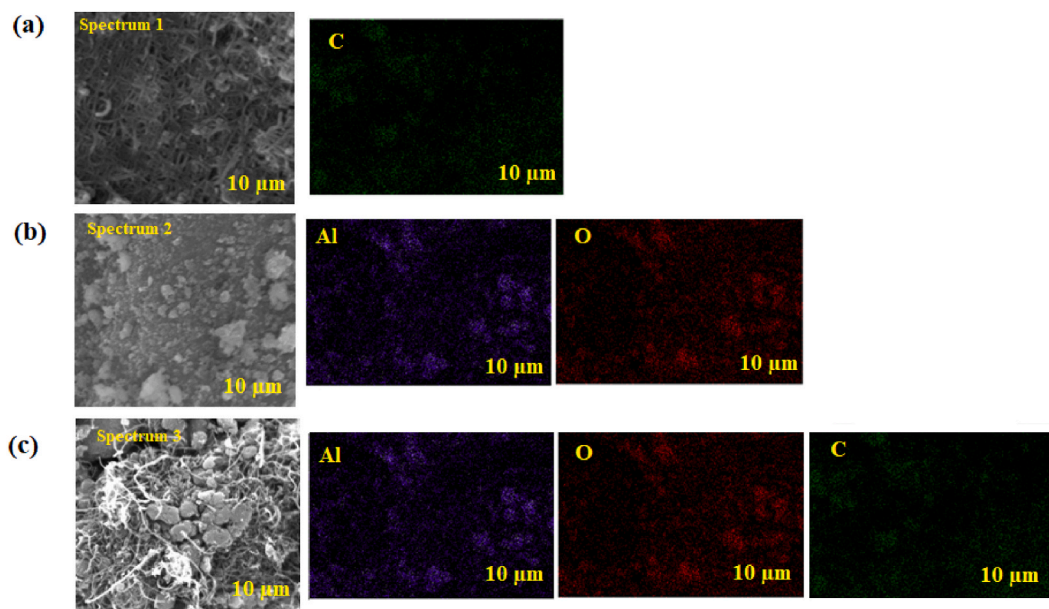


Fig. 6. SEM image, elemental mapping of (a) MWCNTs, (b) $\text{Al}_2\text{O}_3\text{NPs}$, and (c) MWCNTs- $\text{Al}_2\text{O}_3\text{NPs}$.

agreement with the electroactive ion-pair structure.

3.3. Effect of plasticizers

The plasticizer is critical to sensor performance since it is responsible for active component solvation and distribution in the sensor matrix, hence lowering the detection limit and influencing the sensitivity, selectivity, and mobility of the electroactive material molecules in the paste. As a solvent mediator for preparing the suitable paste of the suggested sensors, three synthetic DBS ($\epsilon = 6.4$), DOP ($\epsilon = 5.1$), and *o*-NPOE ($\epsilon = 24$) and two natural olive oil ($\epsilon = 3.06$) and paraffin oil ($\epsilon = 2.13$) plasticizers were used. The results summarized in Table 1 indicated that the carbon paste sensor plasticized with 15 mg of *o*-NPOE exhibited the best potential readings stability with the best Nernstian responses (mV decade^{-1}) and wide range of detection due to its high molecular weight, great polarity, and high dielectric constant of ($\epsilon = 24$).

3.4. Influence of electroactive ion-pair sensitivity

The effect of the electroactive ion-pair on the sensitivity and reproducibility of the sensors was studied (Table 1). Ten carbon paste sensors with different amounts of electroactive ion-pair AC-PM in the range of 5–15 mg have been constructed. The sensors containing 5 mg of AC-PM ion-pair exhibited poor potential readings with slopes -46.8 and -52.6 mV decade^{-1} and linear concentration ranges of 1.0×10^{-4} – 1.0×10^{-3} and 1.0×10^{-6} – 1.0×10^{-3} mol L^{-1} (Sensors 1 and 7). However, the sensor containing 10 mg of AC-PM displayed a remarkable sensitivity towards AC cations with slope -53.5 mV decade^{-1} and -57.1 mV decade^{-1} over concentration

Table 1

Effect of plasticizer on the performance of modified MWCNTs and functionalized MWCNTs- Al_2O_3 nanocomposite sensors.

AC-PM-MWCNTs carbon paste sensor								
No	AC-PM complex (mg)	Plasticizer (115 mg)	Graphite Powder (mg)	MWCNTs (mg)	MWCNTs- Al_2O_3 (mg)	Slope	Linear range mol L^{-1}	r^2
1	5	DBS	250	—	—	-46.8	1.0×10^{-5} – 1.0×10^{-3}	0.9756
2	5	DBS	250	5	—	-48.3	5.0×10^{-5} – 1.0×10^{-3}	0.9875
3	7	DOP	250	10	—	-50.8	1.0×10^{-5} – 1.0×10^{-3}	0.9959
4	10	<i>o</i> -NPOE	250	15	—	-53.5	1.0×10^{-7} – 1.0×10^{-2}	0.9997
5	12	Olive oil	250	5	—	-50.4	1.0×10^{-5} – 1.0×10^{-4}	0.9920
6	15	Paraffin oil	250	10	—	-49.7	1.0×10^{-5} – 1.0×10^{-2}	0.9986
Functionalized AC-PM-MWCNTs- Al_2O_3 nanocomposite carbon paste sensor								
7	5	DBS	250	—	—	-52.6	1.0×10^{-6} – 1.0×10^{-3}	0.9789
8	7	DOP	250	—	5	-54.2	1.0×10^{-6} – 1.0×10^{-3}	0.9899
9	10	<i>o</i> -NPOE	250	—	10	-57.1	1.0×10^{-8} – 1.0×10^{-2}	0.9997
10	12	Olive oil	250	—	5	-55.4	5.0×10^{-7} – 1.0×10^{-2}	0.9988
11	15	Paraffin oil	250	—	10	-53.6	5.0×10^{-7} – 1.0×10^{-2}	0.9968

ranges of 1.0×10^{-7} - 1.0×10^{-2} and 1.0×10^{-8} - 1.0×10^{-2} mol L⁻¹ (Sensors 4 and 9). The modified carbon paste sensors with more than 10 mg AC-MP (12 and 15 mg) exhibited less sensitivity for the detection of AC. This can be attributed to the use of a higher AC-PM ion-pair can cause over-saturation and unsatisfactory characteristics of the sensor as a result of steric hindrance effects at the interface.

3.5. Effect of MWCNTs and MWCNTs-Al₂O₃ nanocomposite

MWCNTs can act as a promoter to enhance the rate of heterogeneous electron transfer of electroactive species and significantly improve the electrical conductivity [43] and surface-to-volume ratio of the MWCNTs and MWCNTs-Al₂O₃ nanocomposite, resulting in increased accumulation of AC molecules on the sensor surface and thus increasing sensitivity and selectivity. As shown in Table 1, various quantities of MWCNTs and MWCNTs-Al₂O₃ nanocomposite range from 0 to 15 mg. The most consistent carbon paste-modified sensor was found to be containing 15 mg of MWCNTs and 10 mg of MWCNT-Al₂O₃ nanocomposite (Sensors 4 and 9). The findings showed that the addition of 15 mg of MWCNT-Al₂O₃ nanocomposite enhanced the sensitivity of the sensor towards the detection of AC with Nernstian -57.107 mV decade⁻¹ and cover a wide concentration range 1.0×10^{-8} - 1.0×10^{-2} mol L⁻¹ and lower the detection limit to 4.8×10^{-9} mol L⁻¹.

3.6. Response time, reversibility, repeatability and reproducibility of modified MWCNTs and factionalized MWCNTs-Al₂O₃ nanocomposite

The average time required to reach a potential within ± 0.1 mV of the final steady-state potential after successive immersions of the electrode in a series of drug solutions of interest (1.0×10^{-8} - 1.0×10^{-2} mol L⁻¹) is used to evaluate sensor response time. The average dynamic response time for the AC-PM-MWCNTs and AC-PM-MWCNTs-Al₂O₃ nanocomposite sensors was determined to be ~ 20 s. Alignment of the fabricated sensors yielded 20 s for the same previous concentration range. The fast response time of the AC-PM-MWCNTs and AC-PM-MWCNTs-Al₂O₃ nanocomposite sensors can be attributed to the significant influence of the electrically conductive material carbon, the overall conductivity of the sensor phase, and the lack of an internal reference solution (Fig. 7a).

The reversibility of the two suggested carbon paste sensors AC-PM-MWCNTs and AC-PM-MWCNTs-Al₂O₃ nanocomposite was evaluated by measuring the potential readings of the sensors using AC drug solutions from high to low (1.0×10^{-2} - 1.0×10^{-8} mol L⁻¹) concentrations.

The finding revealed that the potentiometric behaviors of the designed sensors were reversible (Fig. 7b). The reproducibility of the sensors' potential readings was investigated by carrying out additional measurements of 1.0×10^{-5} mol L⁻¹ AC solution immediately after measuring the first batch of solutions at 1.0×10^{-4} mol L⁻¹ AC. The relative standard deviation for recording emf of six replicate determinations was found 1.2 and 0.47 for AC-PM-MWCNTs and AC-PM-MWCNTs-Al₂O₃ nanocomposite sensors, respectively. This revealed excellent repeatability of the potential response of the sensors.

3.7. Effect of pH

The potentials of the designed suggested carbon paste sensors AC-PM-MWCNTs and AC-PM-MWCNTs-Al₂O₃ nanocomposite sensors were examined for their pH dependence in solutions containing 1.0×10^{-4} mol L⁻¹ AC covering the pH range of 2–10. To modify the acidity of the test solutions, small amounts of (1.0 mol L⁻¹ HCl or NaOH) were introduced in modest amounts, and the potential variation was recorded. Over the pH range of 2–6, which is believed to be the operational pH range of the indicated sensors, the potential response is nearly consistent (Fig. 8). There is a slight discrepancy at pH levels lower than 2, which could be caused by H⁺ interference. At pH values greater than 6, the potential steadily decreased. This decrease could be attributed to the formation of a free

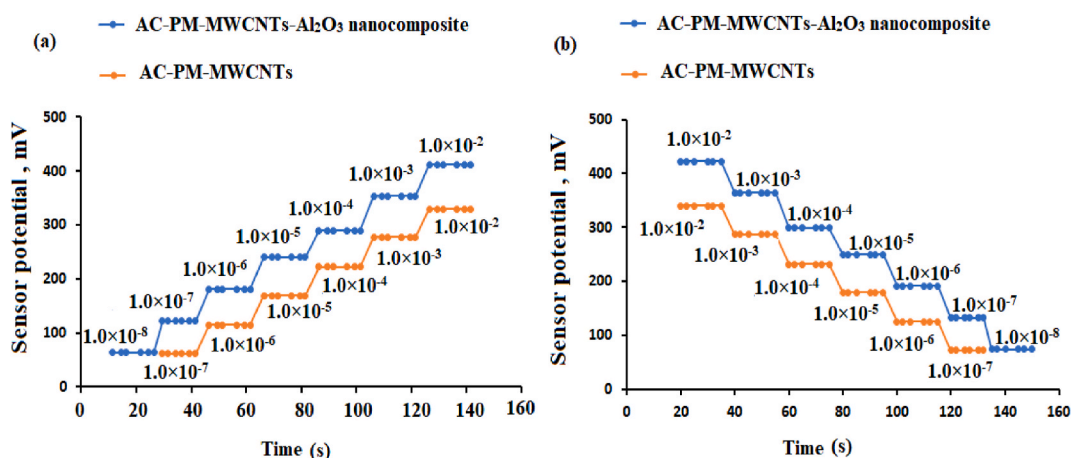


Fig. 7. (A) The dynamic response time of AC-PM-MWCNTs and AC-PM-MWCNTs-Al₂O₃ nanocomposite using AC samples from low to high concentration and (b) The reversibility of AC-PM-MWCNTs and AC-PM-MWCNTs-Al₂O₃ nanocomposite using AC samples from high to low concentrations.

AC base and an increase in OH^- ions in the test solution [9].

3.8. Selectivity of the designed sensors

The selectivity of newly proposed AC-PM-CP, AC-PM-MWCNTs, and AC-PM-MWCNTs- Al_2O_3 nanocomposite sensors for detecting AC^+ ions was investigated using 50 mL of AC solution and foreign materials ($1.0 \times 10^{-3} \text{ mol L}^{-1}$) independently. Cations (Ca^{2+} , Mg^{2+} , Cu^{2+} , Zn^{2+} , Na^+ , K^+ , Cr^{3+} , and Al^{3+}), amino acids (histidine and glycine), sugars (lactose and sucrose), and pharmaceutically prepared additives (talc and magnesium stearate) were among the foreign materials evaluated. The functionalized AC-PM-MWCNTs- Al_2O_3 nanocomposite demonstrated excellent selectivity. Because of the smaller particle size and different physical and chemical properties of metal oxide nanoparticles, the inclusion of Al_2O_3 NPs and MWCNTs improved the selectivity of the sensors for the detection of AC. To characterize the selectivity of proposed AC-PM-MWCNTs and AC-PM-MWCNTs- Al_2O_3 nanocomposite and membrane sensors, the free energy of AC^+ transfer between the aqueous and active sites in the coated membrane is usually used. The tolerable values $\log K_{\text{AC}}^{\text{Pot}}$ were calculated using the following equation (3)

$$\log K_{\text{A,B}}^{\text{Pot}} = E_{\text{B}} - E_{\text{A}} / \text{Slope} + [1 - Z_{\text{A}} / Z_{\text{B}}] \log a_{\text{A}} \quad (3)$$

where ($\log K_{\text{A,B}}^{\text{Pot}}$), E_{A} , and E_{B} are the selectivity coefficients, potentials, and interfering species (equal concentration) of the sensors under consideration. AC activity is represented by a_{A} , whereas AC charges and interfering species are represented by Z_{A} and Z_{B} , respectively. Meanwhile, the equation was utilized to derive the mixed solution approach's selectivity coefficient equation (4).

$$K_{\text{A,B}}^{\text{Pot}} = a'_{\text{A}} - a_{\text{A}} / a_{\text{B}} \quad (4)$$

where a'_{A} is the known AC concentration multiplied by an unknown AC concentration a_{A} . E represents the perspective change. In another test procedure, a known concentration of interfering ion (a_{B}) was introduced to a specified concentration of AC until the same potential was achieved. Potentiometric selectivity coefficients ($K_{\text{AC}}^{\text{Pot}}$) of the fabricated AC-PM-CP, AC-PM-MWCNTs, and AC-PM-MWCNTs- Al_2O_3 nanocomposite sensors were also determined using MSM in the preference of ($1.0 \times 10^{-1} \text{ mol L}^{-1}$) interfering ions. Because of the difference in ionic size, mobility, and permeability of interfering ions compared to AC^+ , no interference was detected (Table 2).

3.9. Quantification of acebutolol hydrochloride

The suggested AC-PM-MWCNTs and AC-PM-MWCNTs- Al_2O_3 nanocomposite sensors were used to detect AC in authentic samples, and the data obtained were evaluated as mean percentage recoveries. Table 3 summarizes the results for the above-mentioned sensors as 98.85 ± 0.6 and 99.67 ± 0.4 , respectively. In comparison to their bulk counterparts, the addition of MWCNTs- Al_2O_3 nanocomposite increased the stability of the sensor. The electrochemical characteristics of a nanocomposite composed of MWCNTs and Al_2O_3 NPs with a high surface area to volume ratio were excellent. The presence of the metal oxide nanocomposite also increases the ion-exchange surface area and improves electron transmission between the inner sensor and the active membrane sites.

3.10. Method validation

Following the ICH recommended principles [44], the validity and applicability of the developed potentiometric systems were

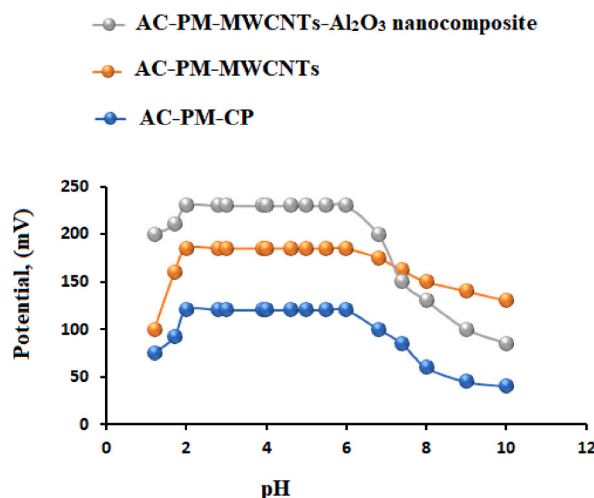


Fig. 8. Effect of pH on the potential reading of AC-PM-CP, AC-PM-MWCNTs, and AC-PM-MWCNTs- Al_2O_3 nanocomposite using $1.0 \times 10^{-4} \text{ mol L}^{-1}$.

Table 2

Tolerable values ($\log K_{AC}^{Pot}$) of the designed AC-PM-MWCNTs and AC-PM-MWCNTs-Al₂O₃ nanocomposite sensors estimated by separate and mixed solution techniques using 1.0×10^{-3} mol L⁻¹ AC and a foreign material (1.0×10^{-3} and 1.0×10^{-1} mol L⁻¹) solution for the two methods, respectively.

Interferents	AC-PM-MWCNTs sensor		AC-PM-MWCNTs-Al ₂ O ₃ nanocomposite sensor	
	SSM	MSM	SSM	MSM
Mg ²⁺	-2.6	-1.4	-3.4	-2.9
Ca ²⁺	-2.4	-2.4	-4.7	-4.3
Ti ⁴⁺	-2.7	-3.4	-4.2	-4.6
Na ⁺	-2.2	-7.1	-3.2	-3.5
Cu ²⁺	-2.1	-9.7	-3.8	-2.8
K ⁺	-2.6	-2.7	-4.6	-4.2
Cr ³⁺	-2.0	-2.1	-3.3	-3.9
Al ³⁺	-2.6	-2.6	-3.2	-2.7
Zn ²⁺	-2.4	-2.5	-3.8	-3.8
Lactose	-2.7	-2.7	-3.5	-4.2
Sucrose	-2.1	-2.1	-4.1	-3.6
Histidine	-2.6	-2.7	-4.2	-5.2
Glycine	-2.9	-2.5	-3.3	-3.4
Magnesium stearate	-2.4	-2.3	-3.6	-3.1
	-2.3	-2.4	-3.1	-4.1

Table 3

The data estimated from the employment of AC-PM-MWCNTs and AC-PM-MWCNTs-Al₂O₃ nanocomposite for the quantification of AC in its authentic samples.

Statistical analysis	AC-PM-MWCNTs sensor			AC-PM-MWCNTs-Al ₂ O ₃ nanocomposite sensor		
	Taken**	Found**	% Recovery	Taken**	Found**	% Recovery
	7	6.96	99.42	8	7.99	99.87
	6	5.97	99.50	6	5.98	99.67
	5	4.93	98.60	5	5.00	100.00
	4	3.97	99.25	4	3.98	99.50
	3	2.95	98.33	3	3.00	100.00
	2	1.96	98.00	2	1.98	99.00
Mean ± SD	98.85 ± 0.6			99.67 ± 0.4		
n	6			6		
Variance	0.36			0.16		
%SE ^a	0.24			0.16		
%RSD	0.61			0.40		

$$^a \text{ SE (\%Error)} = \text{SD} / \sqrt{n} \text{ **Taken and found} - \log [\text{AC}].$$

ensured. AC-PM-MWCNTs-Al₂O₃ nanocomposite and AC-PM-MWCNTs sensors demonstrated linearity of 1.0×10^{-8} - 1.0×10^{-2} and 1.0×10^{-7} - 1.0×10^{-2} , respectively with regression equations $-57.107x + 518.54$ ($r = 0.9996$) and $-53.571x + 423.24$ ($r = 0.9998$) as shown in Fig. 9.

In this study, the limit of detection (LOD) is identified when the potential readings of the proposed AC-PM-MWCNTs and AC-PM-MWCNTs-Al₂O₃ nanocomposite sensors drop by 17.8 mV. The LOD for the two sensors was determined to be 4.8×10^{-8} and 5.0×10^{-9} mol L⁻¹, respectively. To validate the accuracy of the proposed technique, nine AC samples were analyzed utilizing the developed AC-PM-MWCNTs and AC-PM-MWCNTs-Al₂O₃ nanocomposite sensors. The accuracy was summarized in Table 4 and the findings were calculated as 98.68 ± 0.5 and 99.37 ± 0.8 for AC-PM-MWCNTs and AC-PM-MWCNTs-Al₂O₃ nanocomposite sensors, respectively.

The precision of the proposed functionalized sensors was assessed utilizing intermediate precision (intra-day and inter-day) tests. The estimated results were expressed using the relative standard deviation percentage (RSD%). The results were presented in Table 5, and the intra-and inter-day were 0.7 %, 0.9 %, and 0.3 %, 0.3 % for the proposed AC-PM-MWCNTs and AC-PM-MWCNTs-Al₂O₃ nanocomposite sensors, respectively, suggesting excellent precision (<2 %).

The robustness of the designed systems was evaluated by using phosphate buffer to elevate the pH to 7 ± 1 . The results for the aforementioned two sensors were computed to be 98.16 ± 0.5 and $99.760.3$ %, respectively. A different pH meter (Jenway-3510) was utilized to evaluate the robustness of the existing approach. The obtained findings for the tested sensors were 98.25 ± 0.8 % and 99.43 ± 0.3 %. These data revealed that there was no discernible difference between the real and analytical results.

3.11. Assay of the drug in commercial products

AC was evaluated in SPECTRAL® tablets (200 mg AC/tablet) using a direct calibration technique. The computed mean % recoveries of the examined samples utilizing the functionalized AC-PM-MWCNTs and AC-PM-MWCNTs-Al₂O₃ nanocomposite sensors were summarized in Table 6. The AC-PM-MWCNTs-Al₂O₃ nanocomposite sensor displayed higher sensitivity towards the detection of AC

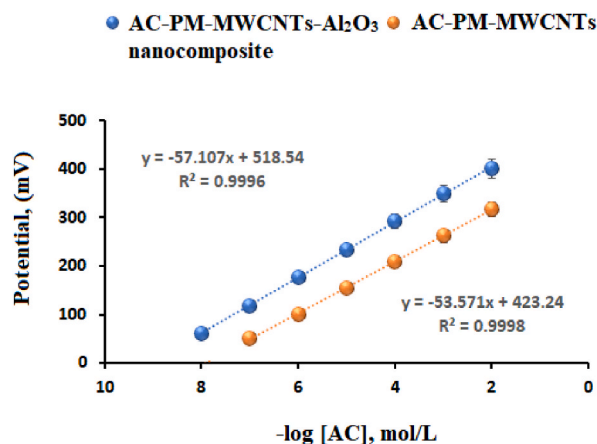


Fig. 9. Calibration graphs of AC-PM-MWCNTs-Al₂O₃ nanocomposite sensor in comparison with AC-PM-MWCNTs sensor.

Table 4

The results of accuracy from the assay of nine authentic AC samples using AC-PM-MWCNTs and AC-PM-MWCNTs-Al₂O₃ nanocomposite sensors.

Statistical analysis	AC-PM-MWCNTs sensor			AC-PM-MWCNTs-Al ₂ O ₃ nanocomposite sensor		
	Taken ^a	Found ^a	% Recovery	Taken ^a	Found ^a	% Recovery
	7	6.95	99.29	8	7.96	99.50
	6.3	6.24	99.05	7.3	7.26	99.45
	6	5.94	99.00	7	7.00	100.00
	5.3	5.25	99.06	6	5.99	99.83
	5	4.92	98.40	5.3	5.27	99.43
	4.3	4.23	98.37	5	4.98	99.60
	4	3.96	99.00	4	4.00	100.00
	3	2.94	98.00	3	2.97	99.00
	2	1.96	98.00	2	1.95	97.50
Mean ± SD	98.68 ± 0.5			99.37 ± 0.8		
n	9			9		
Variance	0.25			0.64		
%SE	0.17			0.27		
%RSD	0.51			0.80		

*SE (%Error) = SD/√ n.

^a Taken and found – log [AC].

Table 5

Findings of precision from the assay of three authentic AC samples using AC-PM-MWCNTs and AC-PM-MWCNTs-Al₂O₃ nanocomposite sensors.

Statistical analysis	AC-PM-MWCNTs sensor					
	Intra-day assay			Inter-day assay		
	Taken*	Found*	% Recovery	Taken*	Found*	% Recovery
	7	6.94	99.14	7	6.95	99.28
	5	4.96	99.20	5	4.92	98.40
	3	2.94	98.00	3	2.92	97.33
Mean ± SD	98.78 ± 0.7			98.34 ± 0.9		
n	3			3		
%RSD	0.71			0.91		
Statistical analysis	AC-PM-MWCNTs-Al ₂ O ₃ nanocomposite sensor					
	Taken*	Found*	% Recovery	Taken*	Found*	% Recovery
	8	7.98	99.75	8	7.96	99.50
	6	5.99	99.83	6	5.98	99.67
	4	3.97	99.25	4	4.00	100.00
Mean ± SD	99.61 ± 0.3			99.72 ± 0.3		
n	3			3		
%RSD	0.30			0.30		

analyte with % recoveries 98.86 ± 0.8 .

The efficient quantification of the target drug was demonstrated by the appropriate functionalization of AC-PM-MWCNTs- Al_2O_3 nanocomposite. This is because the green-produced metal Al_2O_3 NPs have enhanced optical and conductive properties. The increased surface area and reduced particle size improve the interfacial connection between the target ions and the electroactive sites in the coated membrane, improving dynamic responsiveness and sensor stability [45]. The results were compared to those of previously described sensors for determining AC [12]. The results revealed good agreement with no discernible major difference.

Another comparison study was conducted between the functionalized AC-PM-MWCNTs- Al_2O_3 nanocomposite sensor and earlier studies in terms of sensor type, and linear detection range.

The first study in Table 7 proposed the development of a phosphotungstic acid-based plastic membrane sensor to determine the AC sample. The results demonstrated that the suggested sensor's activity spanned the linear concentration range of 1.0×10^{-6} - 1.0×10^{-2} mol L^{-1} . The second study, on the other hand, described the construction of electrochemical sensor-based pencil graphite supported with ethyl cellulose with a linear concentration range of 0.001–200 $\mu\text{mol L}^{-1}$. Further research recommended the use of cerium oxide/graphene nanosheet to create an electrochemical sensor. The measured linear concentration range was determined to be 0.039–486.6 $\mu\text{mol L}^{-1}$. Another study demonstrated the development of a polyvinyl chloride membrane sensor based on sodium tetraphenylborate as the electroactive material. The calculated findings were 6.0×10^{-6} - 4.0×10^{-2} mol L^{-1} . Because of the previously discussed unique qualities of the nanomaterials, the present sensor in this study employing functionalized AC-PM-MWCNTs- Al_2O_3 nanocomposite sensor demonstrates good selectivity, sensitivity, and fast dynamic response [46].

4. Conclusion

In the current work, for sensing a prohibited medication in sports AC in commercial products, highly sensitive, stable, and durable modified carbon paste sensors based on AC-PM-MWCNTs and AC-PM-MWCNTs- Al_2O_3 nanocomposite sensors were used. The electrochemical performance features of the examined MWCNTs such as high surface area, high electrical conductivity, and superior adsorptive character. The factionalized AC-PM-MWCNTs- Al_2O_3 nanocomposite carbon paste sensor shown exceptional and improved AC detection in terms of mean recoveries%, linearity range, detection limit, and precision. In terms of selectivity, the built sensors outperformed current standard sensors in terms of dynamic response. The suggested sensors showed excellent capability and the research laboratories can use this sensor to test AC on a regular basis. The suggested sensor opens up a new sector in the development of nanosensors capable of detecting the lowest amounts of forbidden and toxic substances in routine analysis and quality control studies.

Informed consent statement

Not applicable.

Table 6

Determination of AC concentrations in SECTRAL®200 mg/tablets samples using AC-PM-MWCNTs functionalized AC-PM-MWCNTs- Al_2O_3 nanocomposite sensor.

Statistical analysis	SECTRAL®200 mg/tablets samples						
	AC-PM-MWCNTs sensor			functionalized AC-PM-MWCNTs- Al_2O_3 nanocomposite sensor			
	Taken ^b	Found ^b	% Recovery	Taken ^b	Found ^b	% Recovery	
	7	6.96	99.43	8	7.95	99.38	
	6	5.94	99.00	7	6.93	99.00	
	5	4.93	98.60	6	5.92	98.67	
	4	3.95	98.75	5	4.99	99.80	
	3	2.95	98.33	4	3.96	99.00	
	2	1.95	97.50	3	2.92	97.33	
Mean \pm SD	98.60 \pm 0.7			98.86 \pm 0.8			
n	6			6			
Variance	0.49			0.64			
%SE ^a	0.29			0.33			
%RSD	0.71			0.81			
t-test	1.381 (2.228) ^c			0.637 (2.228) ^c			
F-test	1.44 (5.05) ^c			1.78 (5.05) ^c			
Reported method [12]	99.12 \pm 0.6						
	6						
	0.36						
	0.24						

^a SE (%Error) = %RSD/ \sqrt{n} .

^b Taken and Found-log [AC], mol L^{-1} .

^c The tabulated values of "t" and "F" at confidence level $p = 0.05$.

Table 7

A comparative evaluation between the results obtained from the assay of AC using functionalized AC-PM-MWCNTs-Al₂O₃ nanocomposite sensor and the previously reported sensors.

Analytical Techniques	Reagent	Linearity	Reference
Potentiometric plastic membrane	Phosphotungstic acid	1.0×10^{-6} – 1.0×10^{-2} mol L ⁻¹	[9]
Electrochemical sensor	Pencil graphite supported with ethyl cellulose	0.01–200 μmol L ⁻¹	[10]
Electrochemical sensor	Cerium oxide with graphene nanosheet	0.039–486.6 μmol L ⁻¹	[11]
Polyvinyl plastic membrane	Sodium tetraphenyl borate	6.0×10^{-6} – 4.0×10^{-2} mol L ⁻¹	[12]
Modified CP sensor	AC-PM-MWCNTs-Al ₂ O ₃ nanocomposite	1.0×10^{-8} – 1.0×10^{-2} mol L ⁻¹	Current study

Data availability statement

All data supporting this study are included in the text.

CRediT authorship contribution statement

Amal M. Al-Mohaimed: Investigation, Conceptualization. **Suliman Y. Al Omar:** Supervision, Project administration, Funding acquisition. **Maha F. El-Tohamy:** Writing – original draft, Methodology, Formal analysis, Data curation.

Declaration of competing interest

The authors declare that they have no known competing financial interests or personal relationships that could have appeared to influence the work reported in this paper.

Acknowledgements

The authors extend their appreciation to the Deputyship for Research & Innovation, Ministry of Education in Saudi Arabia for funding this research. (IFKSURC-1-5803).

Appendix A. Supplementary data

Supplementary data to this article can be found online at <https://doi.org/10.1016/j.heliyon.2023.e20997>.

References

- [1] A.J. Schneider, F. Hong (Eds.), *Doping in Sport: Global Ethical Issues*, Routledge, 2020.
- [2] K. Kirby, A. Moran, S. Guerin, A qualitative analysis of the experiences of elite athletes who have admitted to doping for performance enhancement, *Int. J. Sport Pol.* 3 (2011) 205–224, <https://doi.org/10.1080/19406940.2011.577081>.
- [3] J.L. Chappelet, N. Van Luijk, The institutional governance of global hybrid bodies: the case of the World Anti-Doping Agency, *Hybridity in the governance and delivery of public services* 7 (2018) 167–191, <https://doi.org/10.1108/S2051-663020180000007005>.
- [4] S. Wernhart, M. Papatthanasious, T. Rassaf, P. Luedike, The controversial role of beta-blockers in heart failure with preserved ejection fraction, *Pharmacol. Ther.* 243 (2023), 108356, <https://doi.org/10.1016/j.pharmthera.2023.108356>.
- [5] P.D. Chaudhari, A.B. Deore, M.J. Jagtap, D.S. Gupta, Formulation development and evaluation of mucoadhesive buccal tablets of acebutolol hydrochloride, *Asian J. Pharmaceut. Res.* 10 (2022) 34–46, <https://doi.org/10.22270/ajprd.v10i4.1156>.
- [6] V.K. Vashistha, A. Kumar, D.K. Das, S. Alwera, R. Vyas, V. Sharma, S. Sethi, R. Pullabhotla, H. Nagar, Different approaches in thin-layer chromatography for enantioresolution of acebutolol using colistin sulfate as chiral selector, *JPC-J PLANAR CHROMAT* 34 (2021) 211–215, <https://doi.org/10.1007/s00764-021-00109-5>.
- [7] P. Jithavech, P. Suwattananuruk, C. Muangnoi, W. Thitikornpong, P. Towiwat, O. Vajragupta, P. Rojsitthisak, Physicochemical investigation of a novel curcumin diethyl γ -aminobutyrate, a carbamate ester prodrug of curcumin with enhanced anti-neuroinflammatory activity, *PLoS One* 17 (2022), e0265689, <https://doi.org/10.1371/journal.pone.0265689>.
- [8] A. Radha, A. Singh, L. Sharma, K.K. Thakur, Molecular interactions of acebutolol hydrochloride to human serum albumin: a combined calorimetric, spectroscopic and molecular modelling approach, *Mater. Today Proc.* 44 (2021) 1700–1706, <https://doi.org/10.1016/j.matpr.2020.11.872>.
- [9] N.A. Alarfaj, M.F. El-Tohamy, Construction and validation of new electrochemical carbon nanotubes sensors for determination of acebutolol hydrochloride in pharmaceuticals and biological fluids, *J. Chin. Chem. Soc.* 61 (2014) 910–920, <https://doi.org/10.1002/jccs.201300552>.
- [10] A. Yamuna, P. Sundaresan, S.M. Chen, Ethylcellulose assisted exfoliation of graphite by the ultrasound emulsification: an application in electrochemical acebutolol sensor, *Ultrason. Sonochem.* 59 (2019), 104720, <https://doi.org/10.1016/j.ultsonch.2019.104720>.
- [11] S.V. Selvi, N. Nataraj, T.W. Chen, S.M. Chen, P. Balu, X. Liu, Disposable cerium oxide/graphene nanosheets based sensor for monitoring acebutolol in environmental samples and bio-fluids, *J. Environ. Chem. Eng.* 10 (2022), 107182, <https://doi.org/10.1016/j.ultsonch.2019.104720>.
- [12] G.A. Mostafa, M.M. Hefnawy, A. Al-Majed, PVC membrane sensors for potentiometric determination of acebutolol, *Sensors* 7 (2007) 3272–3286, <https://doi.org/10.3390/s7123272>.
- [13] M.C. Carneiro, L.R. Rodrigues, F.T. Moreira, M.G.F. Sales, Colorimetric paper-based sensors against cancer biomarkers, *Sensors* 22 (2022) 3221, <https://doi.org/10.3390/s22093221>.

- [14] S. Sharma, N.P. Shetti, S. Basu, M.N. Nadagouda, T.M. Aminabhavi, Remediation of per- and polyfluoroalkyls (PFAS) via electrochemical methods, *Chem. Eng. J.* 430 (2022), 132895, <https://doi.org/10.1016/j.cej.2021.132895>.
- [15] M. Cuartero, G.A. Crespo, All-solid-state potentiometric sensors: a new wave for in situ aquatic research, *Curr. Opin. Electrochem.* 10 (2018) 98–106, <https://doi.org/10.1016/j.coelec.2018.04.004>.
- [16] N.M. Ivanova, I.V. Podeshvo, M.Y. Goikhman, A.V. Yakimanskii, K.N. Mikhelson, Potassium-selective solid contact electrodes with poly (amidoacid) Cu (I) complex, electron-ion exchanging resin and different sorts of carbon black in the transducer layer, *Sensor. Actuator. B Chem.* 186 (2013) 589–596, <https://doi.org/10.1016/j.snb.2013.06.072>.
- [17] O. Özbek, H. Gezezen, A. Cetin, O. Isildak, A potentiometric sensor for the determination of Pb (II) ions in different environmental samples, *ChemistrySelect* 7 (2022), e202202494, <https://doi.org/10.1002/slct.202202494>.
- [18] Ö. Isildak, O. Özbek, Application of potentiometric sensors in real samples, *Crit. Rev. Anal. Chem.* 51 (2021) 218–831, <https://doi.org/10.1080/10408347.2019.1711013>.
- [19] Z.D. Lin, C.H. Hsiao, S.J. Young, C.S. Huang, S.J. Chang, S.B. Wang, Carbon nanotubes with adsorbed Au for sensing gas, *IEEE Sensor. J.* 13 (2013) 2423–2427, <https://doi.org/10.1109/JSEN.2013.2256124>.
- [20] H. Meskher, C.M. Hussain, A. Thakur, R. Sathyamurthy, I. Lynch, P. Singh, K.H. Tan, R. Saidur, Recent Trends in Carbon Nanotube (CNT) based biosensors for fast and sensitive detection of human viruses: a critical review, *Nanoscale Adv.* 5 (2023) 992–1010, <https://doi.org/10.1039/D2NA00236A>.
- [21] A. Venkataraman, E.V. Amadi, Y. Chen, C. Papadopoulos, Carbon nanotube assembly and integration for applications, *Nanoscale Res. Lett.* 14 (2019) 1–47.
- [22] S. Alim, J. Vejjayan, M.M. Yusoff, A.K. Kafi, Recent uses of carbon nanotubes & gold nanoparticles in electrochemistry with application in biosensing: a review, *Biosens. Bioelectron.* 121 (2018) 125–136, <https://doi.org/10.1016/j.bios.2018.08.051>.
- [23] P.C. Ma, N.A. Siddiqui, G. Marom, J.K. Kim, Dispersion and functionalization of carbon nanotubes for polymer-based nanocomposites: a review, *Composites Part A, Appl. Sci. Manufact.* 41 (2010) 1345–1367, <https://doi.org/10.1016/j.compositesa.2010.07.003>.
- [24] C.M. Gore, J.O. White, E.D. Wachsman, V. Thangadurai, Effect of composition and microstructure on electrical properties and CO₂ stability of donor-doped, proton conducting BaCe_{1-x}(x+y)Zr_xNb_yO₃, *J. Mater. Chem. A* 2 (2014) 2363–2373, <https://doi.org/10.1039/C3TA12668D>.
- [25] A. Akbari, M. Amini, A. Tarassoli, B. Eftekhari-Sis, N. Ghasemian, E. Jabbari, Transition metal oxide nanoparticles as efficient catalysts in oxidation reactions, *J. Nanostruct.* 14 (2018) 19–48, <https://doi.org/10.1016/j.nano.2018.01.006>.
- [26] S. Ganguly, S. Sikdar, S. Basu, Experimental investigation of the effective electrical conductivity of aluminum oxide nanofluids, *Powder Technol.* 196 (2009), <https://doi.org/10.1016/j.powtec.2009.08.010>, 326–230.
- [27] P. Pathak, S. Park, H.J. Cho, Metal oxide semiconductor-carbon nanomaterial network as a flexible chemical sensor for volatile organic compound detection, *IEEE Sensors Applications Symposium (SAS)* (2019) 1–5, <https://doi.org/10.1109/SAS.2019.8705969>.
- [28] C.D. De Souza, B.R. Nogueira, M.E. Rostelato, Review of the methodologies used in the synthesis gold nanoparticles by chemical reduction, *J. Alloys Compd.* 798 (2019) 714–740, <https://doi.org/10.1016/j.jallcom.2019.05.153>.
- [29] Y. Xie, D. Kocaefe, C. Chen, Y. Kocaefe, Review of research on template methods in preparation of nanomaterials, *J. Nanotechnol.* (2016), <https://doi.org/10.1155/2016/2302595>.
- [30] Kaushik Pal, Subhendu Chakraborty, Nibedita Nath, "Limitations of nanomaterials insights in green chemistry sustainable route: review on novel applications" *Green Process, Synth. Met.* 11 (2022) 951–964, <https://doi.org/10.1515/gps-2022-0081>.
- [31] F.E. Ettadili, S. Aghris, F. Laghrib, A. Farahi, S. Saqrane, M. Lahrich, M.A. El Mhammedi, Recent advances in the nanoparticle's synthesis using plant extract: applications and future recommendations, *J. Mol. Struct.* 1248 (2022), 131538, <https://doi.org/10.1016/j.molstruc.2021.131538>.
- [32] A. Molina, M. Al-Sardar, V. Rodriguez-Gonzalez, V. Escobar-Barrios, A.A. Zakhidov, A.I. Mtz-Enriquez, A. Encinas, J. Oliva, Efficient NO₂ detection and the sensing mechanism of stretchable/biodegradable MWCNT based sensors decorated with CeO₂ nanoparticles, *Synth. Met.* 287 (2022), 117091, <https://doi.org/10.1016/j.jphotochem.2018.11.009>.
- [33] V. Manikandan, Jayanthi, P. Priyadharan, A. Vijayarathap, P.M. E. Anbarasan, P. Velmurugan, Green synthesis of pH-responsive Al₂O₃ nanoparticles: application to rapid removal of nitrate ions with enhanced antibacterial activity, *J. Photochem. Photobiol., A: Chem* 371 (2019) 205–215, <https://doi.org/10.1016/j.jphotochem.2018.11.009>.
- [34] H.I. Hamouda, H.M. Abdel-Ghafar, M.H. Mahmoud, Multi-walled carbon nanotubes decorated with silver nanoparticles for antimicrobial applications, *J. Environ. Chem. Eng.* 9 (2021), 105034, <https://doi.org/10.1016/j.jece.2021.105034>.
- [35] G.A. Rance, D.H. Marsh, R.J. Nicholas, A.N. Kholobystov, UV-vis absorption spectroscopy of carbon nanotubes: relationship between the π -electron plasmon and nanotube diameter, *Chem. Phys. Lett.* 493 (2010) 19–23, <https://doi.org/10.1016/j.cplett.2010.05.012>.
- [36] M.H. Penner, *Ultraviolet, visible, and fluorescence spectroscopy*, in: *Food Analysis*, Springer, Cham, 2017, pp. 89–106.
- [37] R.A. Ismail, S.A. Zaidan, R.M. Kadhim, Preparation and characterization of aluminum oxide nanoparticles by laser ablation in liquid as passivating and anti-reflection coating for silicon photodiodes, *Appl. Nanosci.* 7 (2017) 477–487, <https://doi.org/10.1007/s13204-017-0580-0>.
- [38] J. Jana, M. Ganguly, T. Pal, Enlightening surface plasmon resonance effect of metal nanoparticles for practical spectroscopic application, *RSC Adv.* 89 (2016) 86174–86211, <https://doi.org/10.1039/C6RA14173K>.
- [39] S. Lu, X. Wang, Z. Meng, Q. Deng, F. Peng, C. Yu, X. Hu, Y. Zhao, Y. Ke, F. Qi, The mechanical properties, microstructures and mechanism of carbon nanotube-reinforced oil well cement-based nanocomposites, *RSC Adv.* 46 (2019) 26691–26702, <https://doi.org/10.1039/C9RA04723A>.
- [40] K.A. Attia, A.M. Abdel-Raouf, A. Serag, S.M. Eid, A.E. Abbas, Innovative electrochemical electrode modified with Al₂O₃ nanoparticle decorated MWCNTs for ultra-trace determination of tamsulosin and solifenacin in human plasma and urine samples and their pharmaceutical dosage form, *RSC Adv.* 12 (2022) 17536–17549, <https://doi.org/10.1039/D2RA01962K>.
- [41] A. Saravanan, K. Prasad, N. Gokulakrishnan, R. Kalaivani, T. Somanathan, Efficiency of transition metals in combustion catalyst for high yield helical multi-walled carbon nanotubes. *Advanced science, Tissue Eng. Regen. Med.* 6 (2014) 809–813, <https://doi.org/10.1166/ase.2014.1569>.
- [42] S. Kumar, V.D. Mote, R. Prakash, V. Kumar, X-ray analysis of α -Al₂O₃ particles by Williamson–Hall methods, *J. Mater. Sci.* 5 (2016) 545–549, <https://doi.org/10.1166/mat.2016.1345>.
- [43] X. Chen, A.J. Gross, F. Giroud, M. Holzinger, S. Cosnier, Comparison of commercial and lab-made MWCNT buckypaper: physicochemical properties and bioelectrocatalytic O₂ reduction, *Electroanal.* 7 (2018), <https://doi.org/10.1002/elan.201800136>, 1511–1120.
- [44] S.K. Branch, Guidelines from the international conference on harmonisation (ICH), *J. Pharm. Biomed. Anal.* 38 (2005) 798–805, <https://doi.org/10.1016/j.jpba.2005.02.037>.
- [45] S.Y. Al Omar, A.M. Al-Mohaimed, M.F. El-Tohamy, Ultrasensitive functionalized CeO₂/ZnO nanocomposite sensor for determination of a prohibited narcotic in sports pethidine hydrochloride, *Heliyon* 9 (2023), e15793, <https://doi.org/10.1016/j.heliyon.2023.e15793>.
- [46] P. Mishra, U. Singh, C.M. Pandey, P. Mishra, G. Pandey, Application of student's t-test, analysis of variance, and covariance, *Anaesthesia* 22 (2019) 407.